ADVANCED ELECTRONIC MATERIALS
www.advelectronicmat.de

Highly Stretchable Conductors Made by Laser Draw-Casting of Ultralong Metal Nanowires

Kaihao Zhang, Kewen Han, Shengtai Shi, Gaurav Bahl, and Sameh Tawfick**

Compliant conductors with large stretching and bending capabilities are enabling novel flexible energy devices, epidermal electronics, and medical implants. They comprise micro- or nanoscale conductive network supported on a compliant substrate. They are commonly fabricated by physical vapor deposition of thin and mechanically fragile metal films, or coating with short percolating nanowire networks, and therefore suffer from trade-offs between maximum stretchability and conductivity. Here, we report the fabrication of robust highly stretchable conductors which afford up to 700% strain with less than 0.4% change in resistivity using ultralong (aspect ratio of 10^5) high-quality palladium (Pd) wires buckled on the surface of a compliant substrate. This high performance is achieved owing to a newly developed laser draw-casting (LDC) process where a fused silica capillary is heated by laser and drawn at a rate of 0.4 m s^{-1}, while a Pd wire is simultaneously cast to fill the capillary. We can currently achieve wire diameters ranging from 250 nm to a few microns and several centimeters length. Without annealing or postprocessing, the wires have high-quality crystalline structure, high conductivity of 7.1×10^6 S m^{-1} and high ductility to withstand in-plane buckling into creases and ridges without fracture. This leads to a figure of merit (defined as mechanical strain divided by the relative change in conductivity) of 1801.

Several configurations of stretchable electronic materials have recently been designed based on "curvy" patterns which enable thin metallic lines to stretch, bend, and deform into complex shapes without breaking by maintaining small local strains.[1–3] For example, stretchable composite conductors have been developed based on the percolation networks of discrete conductive nanobuilding blocks, such as metallic nanowires or carbon nanotubes (CNTs) on elastomeric substrates, where enhanced stretchability effects can also be magnified by local sliding.[4,5] Flexible CNT networks are prepared by spin-coating or vacuum filtration and transfer, where strains up to 700% were reached.[3] However, the electrical conductivity drops by about two orders of magnitude per 100% strain.[6] This is a common disadvantage in percolation network films, where, in addition to hysteresis caused by contact resistance, conductivity is often lost as a result of lack of local uniformity or due to loss of contact.[4] Other designs employ photolithography to precisely define continuous conductive lines with deterministic curvatures as shown by Rogers and co-workers,[7–9] leading to minimization of local strains with respect to the macroscale conductor deformation. These flexible electrical devices can reach strains of ≈100%, but involve a series of complex fabrication steps including photolithography, e-beam or sputtering deposition, and lift-off.

The performance of stretchable conductor films also depends on the structural quality of the conductive elements. For example, while CNTs are theoretically as conductive as metal films and wires, they have demonstrated only moderate specific conductivity due to short lengths and large defect density caused during synthesis, purification, and functionalization. Metallic thin films and nanowires made by vacuum physical vapor deposition, such as electron beam evaporation or sputtering, intrinsically offer higher electrical performance in stretchable and foldable electronics. However, their implementation is limited by the cost of vacuum processing for large area applications, and their poor mechanical properties due to the ultrafine-grain structure which make them brittle and prone to fracture and cracks. Solution-synthesized silver and gold nanowires[10,11] are also attractive for percolation networks. However, short (1–20 μm) nanowires[12] suffer from local contact losses and hysterisis at large strains. Recently, a hybrid multiscale design incorporating microscale diameter and centimeter-long metal wires has been used with nanoscale percolation networks to enhance the conductive performance under strain.[13–16]

In this work, we report a new route to fabricate long metal micro- and nanowires by a novel laser-assisted draw-casting process, and demonstrate their integration in highly stretchable conductors reaching 700% strain while maintaining almost invariant electrical conductivity. Using this new process, Pd wires with submicron diameters and centimeter length are individually drawn at speeds close to 0.4 m s^{-1}. In particular, these wires represent a new route to the fabrication of high performace and reliable stretchable conductors which overcome the limitations associated with thin films or percolation networks. The throughput of the wire manufacturing is scalable. While the drawing speed is limited by our current actuators, we expect that this approach can be implemented in a high throughput manufacturing setting, where bundles of wires can be drawn in parallel at speeds of several meters per second. We demonstrate a simple route to laminate the wires on flexible substrate and measure their strain-dependent electrical conductivity. We show that as-drawn Pd wires have superior electrical conductivity and can accommodate large strains by affording higher local buckling modes without fracture.

We fabricate the Pd nanowires by the LDC process to achieve a smaller diameter range than what could be reached

K. Zhang, K. Han, S. Shi, Prof. G. Bahl,
Prof. S. Tawfick
Mechanical Science and Engineering
University of Illinois Urbana-Champaign
Urbana, Illinois 61801, USA
E-mail: bahl@illinois.edu; tawfick@illinois.edu

DOI: 10.1002/aelm.201600003

ADVANCED ELECTRONIC MATERIALS
www.advelectronicmat.de

Materials Views
www.MaterialsViews.com

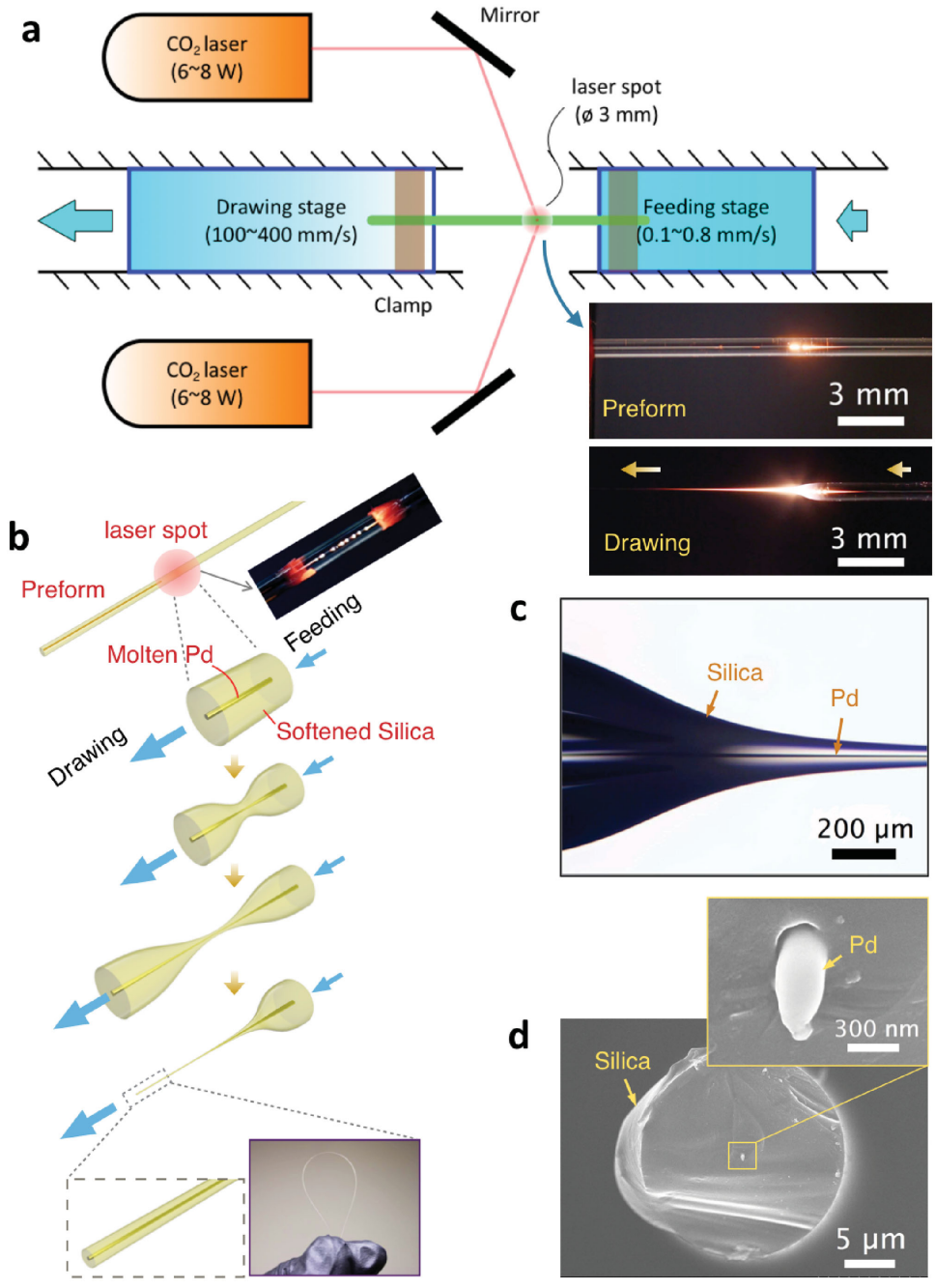

Figure 1. Fabrication setup, process, and results of Pd nanowire using the laser-assisted draw-casting (LDC) method. a) Schematic of the LDC setup showing the laser heating and drawing stages. Photographs on the right show the heated (top) and drawn (bottom) preform. b) Schematics of LDC process and picture of the as-drawn Pd wire embedded in the silica capillary. c) Optical image of the reduced area in the drawn capillary meniscus with the Pd wire inside. d) Scanning electron microscope (SEM) image showing the cross section of the as-drawn Pd wire embedded in the silica cladding.

with traditional metal wire drawing dies. This process is different from the "Taylor process,"[17–20] which has been recently used by Bayindir et al.[21] and other researchers to fabricate multimodal and multifunctional optical fibers and metal nanowires.[22–24] Notably, our process operates at temperatures exceeding 1700 °C, and speeds close to 400 mm s^{-1} where the fused silica capillary is drawn at its glass transition temperature while the metal is molten and cast into the capillary's core.

In the LDC process, we start from a commercially available Pd wire of 25.4 μm in diameter and manually insert it inside a fused silica capillary (ϕ ID: 50 μm, ϕ OD: 800 μm, $L \approx 40$ mm) as shown in **Figure 1**a. The Pd was chosen here since (1) it has high electrical conductivity, (2) offers electrochemical sensitivity (including hydrogen detection), and (3) possesses a melting point close to the softening point of silica capillary which makes it suitable for the processing conditions in LDC. The

Pd/silica preform is fixed to two motorized linear actuators by bolted clamp assemblies. Two CO_2 laser beams intersect on the preform and preheat it to the elevated temperatures, at which silica capillary softens (softening point ≈1943 K) and the Pd core melts (melting point ≈1828 K). These temperatures have been confirmed by attaching thermocouples to the outside of the silica tube and calculating the rate of heat flux and temperature gradient across the tube. As illustrated in Figure 1b, the molten Pd core tends to bead up to minimize its surface energy before it fills the spacing of the silica capillary as the drawing motion starts.[25] As a result, the molten Pd is sealed within the softened silica capillary in the initial preheating phase, and the drawing forces are transferred by shear stresses at the inner silica walls. We choose the preheating power and dwelling time so that the silica viscosity becomes low enough to enable high drawing rates and significant reduction in the Pd wire diameter in one drawing step. The process can be qualitatively described as follows. The softened silica mold forms a conical-shaped meniscus due to tangential hoop and axial stresses while maintaining high enough viscosity and confining the flow of Pd melt. The profile evolution of the silica tube as a function to the drawing temperature and velocity in the meniscus (soft) region can be predicted by Navier–Stokes equation.[26,27] Since the viscosity of the softened silica is around 10^8 times of that of the molten Pd at the drawing temperature, the effect from the Pd melt on silica conical profile is negligible. The silica mold hence forms a dynamic mold into which the molten metal is cast. More specifically, the shear stresses at the silica–Pd interface stretch drive and form the Pd melt, which simultaneously fills the inner diameter. Capillary forces of the molten metal are of higher importance as they either assist or resist the filling process based on the interfacial interactions. Thus, during the drawing process, the metal is cast into a thin fiber strand before it solidifies. The volume of stretched capillary and fiber is balanced by the continuous feeding of preform at low speeds (<0.8 mm s^{-1}) from the input side. Figure S1 (Supporting Information) depicts the experimental process and Tables S1 and S2 of the Supporting Information list the materials and typical process parameters used in LDC. To confirm the mechanism of the process, we used a thermocouple to measure the temperature at the outer wall and found it to be 1868 K, which is in the range of the glass transition of pure fused silica (≈1900 K). We note that the measured wall temperature is considered lower bound of the silica temperature due to losses associated with the thermocouple contact resistance. We also measured and calculated the temperature gradient through 370 µm wall thickness and found the heat flux to be 161 kW m^{-2} and that the maximum temperature gradient to be 128 K. The lower bound for the temperature of the Pd wire is hence 1740 K which is 95% of the melting temperature.

Notably, similar to commercial continuous casting of metal slabs (e.g., steel), the silica tube has significantly higher viscosity than the molten metal and acts as a supporting scaffold guiding the flow of the low-viscosity metallic core.[28,29] As shown in Figure 1c, during this draw-casting process, the silica capillary takes the shape of a conical meniscus and restricts the Pd core flow until the fiber dimensions are frozen. Therefore, the geometry of the drawn Pd wire can be precisely designed only by controlling the reduction in the capillary inner diameter. This simple understanding allows us to precisely tune the wire continuity and diameter.

The LDC process represents a novel cost-efficient and scalable metallic micro- and nanowires manufacturing process. The geometry of drawn metal wires can be controlled by the process parameters. The highest aspect ratio wire obtained had ≈140 mm length and a diameter of 250 nm (aspect ratio exceeding 10^5) encapsulated in the silica mold. The thinnest diameter that we can currently achieve in one drawing step is limited by the maximum speed of our actuator setup (0.4 m s^{-1} as discussed in the Supporting Information). We use hydrofluoric acid (HF) etching to dissolve silica mold and obtain bare Pd nanowires (see the Methods section in the Supporting Information). **Figure 2**a shows a typical as-drawn Pd wire deposited on a silicon substrate. Since we use a linear stage of fixed travel length, the conical shape of silica meniscus is transferred to the Pd wire leading a tapered morphology with negligible surface roughness. For the shown wire, the diameter varies from 1203 to 180 nm over 3.75 mm length along the wire, indicating ≈2.73 Å µm^{-1} taper angle and aspect ratio of ×10^4. The microscopic morphologies at different positions of the wire are illustrated in Figure 2b.

During the drawing process, a decrease in the inner diameter of the capillary takes place downstream of the laser spot, where the temperature is the highest. We observed that the preform feeding rate strongly affects the wire diameter and follows mass conservation laws. As presented in Figure 2c, the silica meniscus length L_m, which denotes the distance from where the necking starts to where the silica dimensions are frozen, decreases with the lower preform feeding rate. As a result, the inner diameter of the capillary gets smaller with low preform feeding, leading to the thinner Pd wires. Therefore, the diameter of the wires can be controlled through varying the preform feeding rate.

We studied the size effect on the electrical conductivity of these wires, to quantify the deviation from bulk conductivity caused by electron scattering at the surface and grain boundaries.[30] We measured the electron transport in the drawn Pd wires by the four-probe method. **Figure 3** presents the dependence of the wire conductivity on its diameter, and the inset shows the representative *I–V* curves for the commercially procured Pd wire and the as-drawn one. We observe that the electrical conductivity of Pd wires drops by 15.5% while the diameter decreases by 98.8%. The conductivity of a 1.26 µm diameter wire is ten times higher than the best single-walled CNT fibers[31] (made from wet spinning by the Behabtu et al.) and 100 times greater than the highest-quality aligned multiwalled CNT films (typically below 10^4 S m^{-1}).[32] We use electron back scattering diffraction to confirm the formation of crystals spanning the entire cross section of the wires in a bamboo-shaped grain structure (Figures S3 and S4 of the Supporting Information).[24,33,34] Notably, these measurements are made on the wires as drawn (without any subsequent thermal annealing).

The buckling behavior of the Pd wires on prestrained elastomeric substrates is studied, toward their use in flexible conductors. Here, 3M VHB (Very High Bonding) tapes are used as the flexible substrate because they are transparent and can accommodate uniaxial prestrain up to 830% ($\varepsilon_{pre} = \Delta L/L \approx 830\%$)

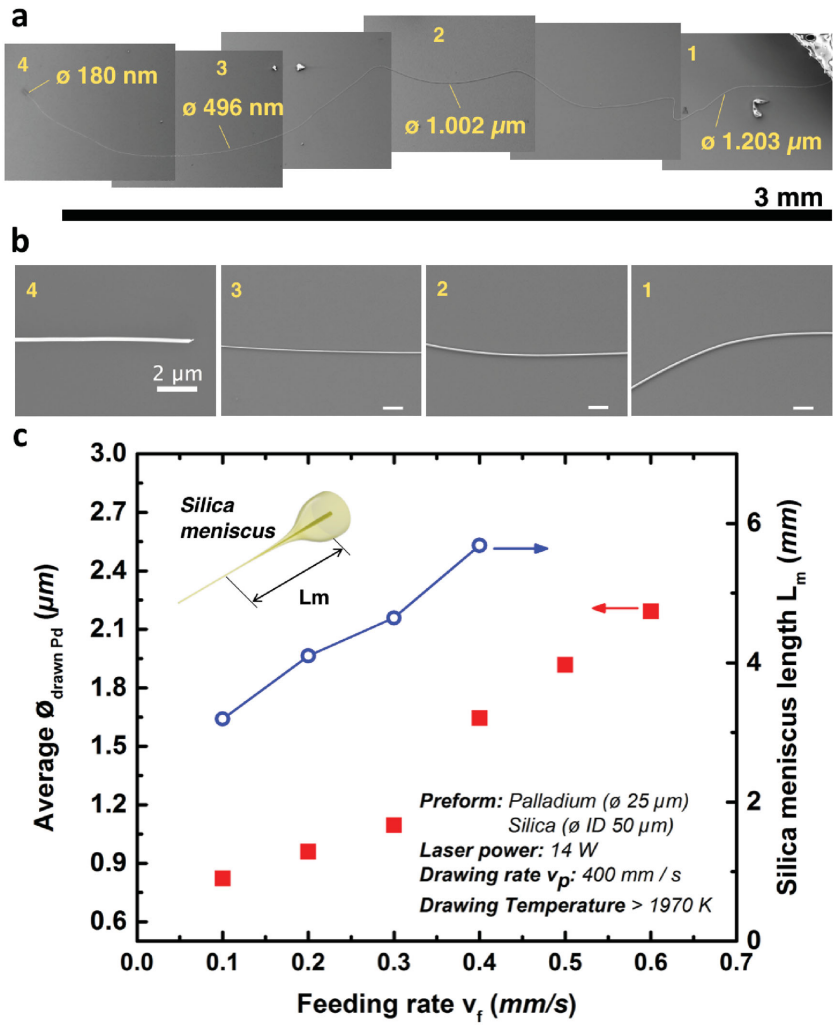

Figure 2. Taper morphology and diameter control of Pd wires. a) Stitched SEM images of a bare Pd wire on the silicon substrate. b) SEM images of the Pd wire at the different positions. c) Measured average Pd diameter and silica tapered meniscus length as a function of varying the feeding rate.

without tearing. The silica-coated Pd wires are deposited and aligned on the prestretched substrate, followed by etching of the silica with HF, to which VHB is notably resistant. We observe unique buckling behavior of the Pd wires, and in particular a transition from elastic to plastic buckling. **Figure 4** shows a schematic and scanning electron microscope (SEM) images of the buckling transformation from sinusoidal to zigzag pattern which occurs as soon as buckling is initiated. This peculiar pattern is indicative of inelastic buckling of Pd wires. The elastic buckling wavelength (λ) of elastic wires on an elastomeric substrate can be described by[35]

$$\lambda \approx \frac{14\pi}{5}\left(\frac{E_w I}{E_s}\right)^{1/4} \quad (1)$$

where E_w and E_s are the wire and substrate moduli, respectively, and I is the second moment of area of the wire. The elastic buckling is hence independent of the value of prestrain for small strains. We found that we can adopt this equation to predict the inelastic buckling of wires of various diameters and at different prestrains simply by using the measured E_w, which equals 58 GPa, a value smaller than the theoretical Young's modulus of bulk Pd (121 GPa) (Figure 4b). This is, in principle, similar to using the tangent modulus to calculate the critical load for inelastic buckling and the formation of a plastic hinge.[36] Qualitatively, when the compressive strains on the concave side of a slender buckling element exceeds the elastic strain limit, a plastic hinge is formed where the modulus is effectively reduced, following the decrease of the stress–strain slope postyielding. For inelastic buckling columns, it has been shown that the local slope, known as the tangent modulus, accurately predicts the onset of buckling. As buckling progresses, the effective modulus is increased as strain reversal occurs on the convex side of the buckling wire where the stresses gradually change from being compressive to tensile. The effective modulus of the Pd wire hence evolves as the substrate is released in inelastic buckling, and is a function of both the prestrain and instantaneous strain. Regardless of whether a substrate is present (such as in our experiments) or not (such as in columns compression testing), the formation of plastic hinge is associated with energy dissipation, and the straightening of the wire profile from a sinusoidal geometry to straight beams connected by a small radius elastic hinge. A precise description of this phenomenon will be presented in a future study.

We investigate the upper limit of prestretch prior to depositing the wire to achieve the highest possible stretchability, and to relate the buckling mechanics to the electrical conductivity. **Figure 5**a depicts the fabrication process of the proposed stretchable conductor. As-drawn silica-coated Pd wire with average diameters ≈1.5–2.5 μm was cut into 30 mm long pieces. Since the silica cladding has the diameter around 30 μm, it is easy to handle and pattern those pieces on the elastomeric substrate. Then the 830% prestrain is released to the initial length, and the Pd microwires formed high-order in-plane buckling patterns (including creasing and twisting loops) on the substrate, as depicted in schematics in Figure 5b. This pattern is different from the purely elastic sinusoidal buckling (observed by others at strains on the order of 100%),[1,35] as well as the zigzag buckling pattern observed for our wires at strains of 50%. We observed the buckling evolution as the strains are released and note three modes of evolution: (i) some buckles initially form sinusoidal patterns that grew in amplitude; (ii) as buckling proceeds beyond the elastic range, the sinusoidal geometry is transformed to zigzag-like pattern indicative of inelastic buckling and the formation of a plastic hinge, (iii) some of the buckles locally develop into higher-order

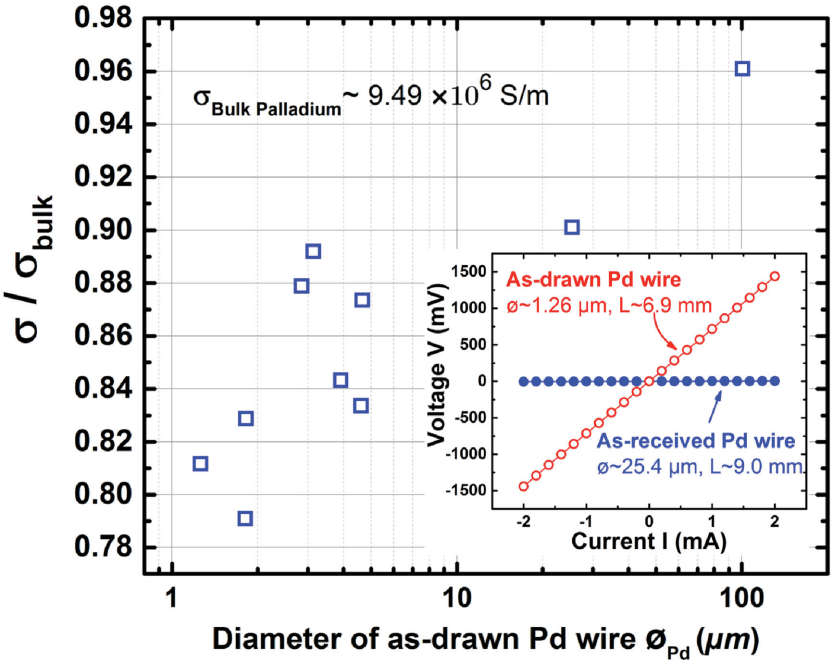

Figure 3. Electrical conductivity of as-drawn Pd wires relative to the bulk for wire diameters ranging from 1–100 μm average diameter. Notably, the wires are tapered; and the reported average diameter is measured at the middle of the length. The diameter reaches 200 nm on the thin end. The inset shows the linear characteristic of the *I–V* curve for a typical Pd wire.

buckling modes, including intricate folding, creasing, and self-intersecting configurations;[37,38] and (iv) as buckling evolves further, wrinkles adjacent to the higher-order buckles decay in both amplitude and wavelength. The observed buckles result from the interaction of the large local strain, adhesion to the substrate with the intrinsic material's crystalline structure orientation. Similar transition from a simple wavy buckling to the localized folding and intersecting pattern has been observed in thin elastic membranes by at large strains, and is known as fold–crease transition.[39–41] Figure 5b shows optical images of the zigzag buckling pattern with periodic folds and self-intersections of the compressed Pd wire on the released VHB substrate. Importantly, we have observed that wires with diameter smaller than or equal to 5 μm buckle in plane, while those of larger diameter buckle out of plane, as governed by the competition between bending strain energy and surface adhesion. Figure S4 (Supporting Information) depicts these in-plane buckling patterns and Pd–VHB interface. The wires do not break even at local strains exceeding 53%, as measured by the radius of curvature. Notably, several recent studies have shown that single-crystalline metal nanowires usually exhibit promising mechanical properties, including up to 50% elastic tensile strains in single-crystalline Cu nanowire,[38] and pseudoelastic behaviors with recoverable strains of 50% in Pd nanowires.[41] As a result, LDC fabricated wires enable an order of magnitude larger strains than short nanowires (e.g., compared to 6.4% for Si nanowire).[42] We have measured the change in resistivity when the conductor is subject to cyclic strain and have not observed any noticeable difference (Figure S7, Supporting Information).

We demonstrate the straightforward integration of the wires to fabricate stretchable electrical wiring for a light-emitting diode (LED). Buckled Pd microwires are patterned on a VHB substrate as illustrated in Figure 5c and re-stretched up to 220% without any observable difference in LED luminance. This strain is limited by the pop-up stability of the LED on the stretched elastomer. We measure the change in resistivity of as-fabricated Pd wire/VHB sample under strains from 100% to 700% (Figure 5d) by mounting a linear translation stage on two-point probe setup. Galinstan, a gallium–indium–tin eutectic that is liquid at room temperature, is used to connect the patterned Pd microwire and copper electrodes. The drawn Pd wires used

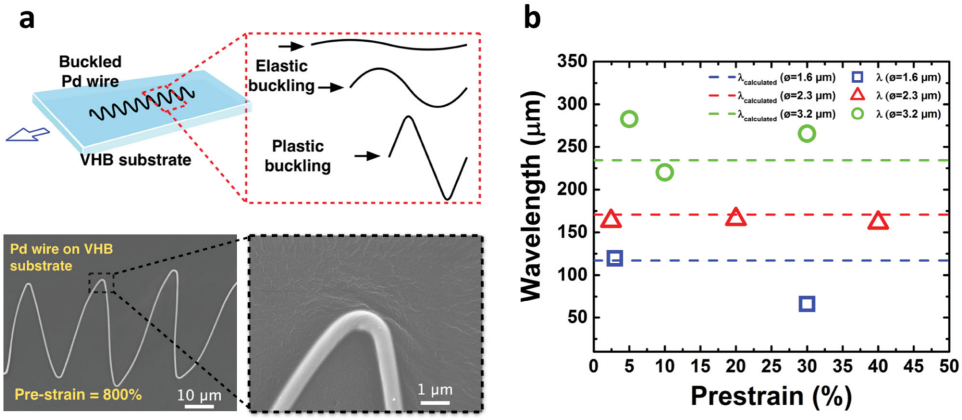

Figure 4. Buckling analysis of Pd wires at various prestrains. a) Schematic of the buckling of Pd wire on a prestrained VHB tape transitioning from sinusoidal elastic buckling to inelastic buckling patterns at larger prestrains as shown in the SEM image. b) Elastic buckling wavelength measured for wire diameters of 3.3 μm (green circles), 2.3 μm (red triangles), and 1.6 μm (blue squares). The horizontal dash lines show the buckling wavelength as described by Equation (1).

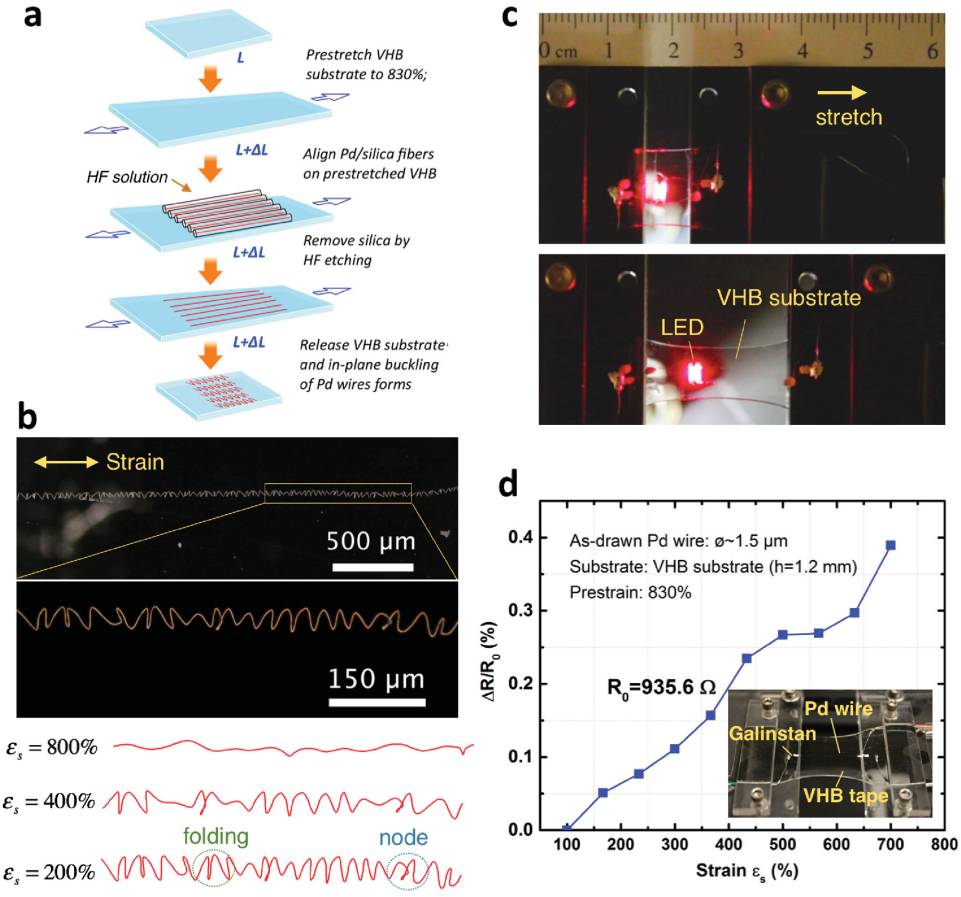

Figure 5. Fabrication processes and characterization of the stretchable conductor based Pd wires deposited on a VHB thin film. a) Process to deposit and etch the Pd wires on a prestretched VHB substrate (initial strain >800%). b) Optical photograph of buckling of the ultralong Pd wire as the prestretch is released to 200% strain (top two frames), and extracted buckling geometry evolution at variable strain levels to show the higher-mode folding and nodes (bottom three frames). c) Photographs of stretched LED circuit on VHB substrate. d) Resistance variation with strain under unidirectional stretching.

for this simple circuit have a length of 25 mm and an average diameter of 2.5 μm. The resistance is measured under constant strain conditions using a two-probe resistance meter (Keysight 34465A). During stretching, the wrinkled Pd wire reduces its buckling amplitude but maintains continuity on the surface of VHB substrate. The conductivity slightly decreases with strain, dropping by only 0.4% at 700% strain. This conductive performance is superior by an order of magnitude compared to other stretchable conductors. **Figure 6** compares the performance of as-fabricated Pd/VHB conductor with other stretchable electronics such as randomly percolation networks of CNTs/graphene. The mechanical strain divided by the relative change in conductivity (or resistivity) represents the "figure of merit" of stretchable conductors. While the material used in this work (VHB) can only be stretched to 800%, the performance of the Pd wires shows a figure of merit of 1801, which is threefold the highest reported value of 592 recently reported by Liu et al.[3]

In summary, we developed a new process to fabricate centimeter-long Pd micro- and nanowires and demonstrated their integration in a highly stretchable conductor having a figure of merit of 1801, with the maximum stretchability of 700%. This demonstrates a new route to making high performance stretchable conductors. This novel LDC process can also enable the fabrication of a variety of metal wires for a wide range of applications, and, due to its high rates (≈m s^{-1} drawing speed) is suitable for high throughput production. Geometry of the drawn fiber is tunable via controlling the preform properties and process parameters. A 140 mm long silica-coated Pd wire with diameter as small as 250 nm was obtained in our experiments, leading to an aspect ratio of $>10^5$. According to our experiments and calculations, the diameter scales inversely with the drawing speed, and we can achieve wires of ≈10 nm at a drawing speed of 5 m s^{-1} and higher laser power. We demonstrate that as-drawn Pd microwires exhibit excellent mechanical and electrical performance. In particular, a highly stretchable electrical conductor exhibits record-breaking resistance change of less than 0.4% when the substrate is strained up to 700%. To the best of our knowledge, the performance of proposed stretchable conductor is superior to most of the CNT/Ag NW-based interconnects or sensors, which are restricted by high junction resistance in NW network or low mechanical strength of patterned structures. We believe that the ultralong ultra-high-aspect-ratio metal nanowires fabricated by LDC are promising for applications in flexible and wearable electronics,

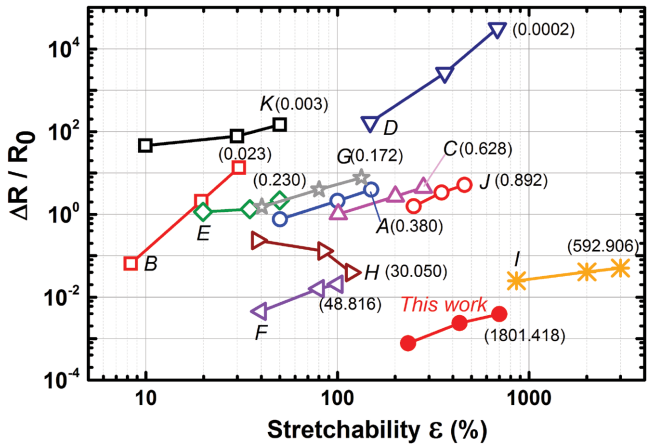

Figure 6. "Figure of merit" of recently reported stretchable conductors. A: CNT network sprayed on Polydimethylsiloxane (PDMS),[4] B: graphene films on PDMS,[43] C: aligned CNT thin films on PDMS,[44] D: CNT thin films sprayed on VHB substrate,[6] E: CNT–polymer composite,[45] F: aligned CNT ribbons embedded in PDMS,[46] G and H: CNT–polymer composite gel coated on PDMS,[5,47] I: multilayer CNT sheath wrapped on a rubber fiber core,[3] J: Ag nanowire networks on Eco-flex substrate,[14] K: Au nanotrough networks on PDMS substrate.[48] The numbers in brackets show $\frac{\varepsilon}{\Delta R/R_0}$ at the maximum strains.

as well as transparent conductive devices, as well as fundamental metallurgical studies of nanoscale wire mechanical and electrical behavior.

Supporting Information

Supporting Information is available from the Wiley Online Library or from the author.

Acknowledgements

All authors acknowledge funds from the department of Mechanical Science and Engineering at the University of Illinois at Urbana-Champaign. S.T. and K.Z. acknowledge partial support from US Office of Naval Research (ONR) grant N00014-15-1-2469 (Dr. Ignacio Perez). G.B. and K.H. acknowledge partial support from the US National Science Foundation through grant ECCS-1509391.

Received: January 4, 2016
Revised: February 17, 2016
Published online: April 9, 2016

[1] J. A. Rogers, T. Someya, Y. G. Huang, *Science* **2010**, *327*, 1603.
[2] D. H. Kim, R. Ghaffari, N. S. Lu, J. A. Rogers, *Annu. Rev. Biomed. Eng.* **2012**, *14*, 113.
[3] Z. F. Liu, S. Fang, F. A. Moura, J. N. Ding, N. Jiang, J. Di, M. Zhang, X. Lepro, D. S. Galvao, C. S. Haines, N. Y. Yuan, S. G. Yin, D. W. Lee, R. Wang, H. Y. Wang, W. Lv, C. Dong, R. C. Zhang, M. J. Chen, Q. Yin, Y. T. Chong, R. Zhang, X. Wang, M. D. Lima, R. Ovalle-Robles, D. Qian, H. Lu, R. H. Baughman, *Science* **2015**, *349*, 400.
[4] D. J. Lipomi, M. Vosgueritchian, B. C. K. Tee, S. L. Hellstrom, J. A. Lee, C. H. Fox, Z. N. Bao, *Nat. Nanotechnol.* **2011**, *6*, 788.
[5] T. Sekitani, Y. Noguchi, K. Hata, T. Fukushima, T. Aida, T. Someya, *Science* **2008**, *321*, 1468.
[6] L. B. Hu, W. Yuan, P. Brochu, G. Gruner, Q. B. Pei, *Appl. Phys. Lett.* **2009**, *94*, 161108.
[7] D. Y. Khang, J. A. Rogers, H. H. Lee, *Adv. Funct. Mater.* **2009**, *19*, 1526.
[8] C. H. Lee, Y. J. Ma, K. I. Jang, A. Banks, T. Pan, X. Feng, J. S. Kim, D. Kang, M. S. Raj, B. L. McGrane, B. Morey, X. Y. Wang, R. Ghaffari, Y. G. Huang, J. A. Rogers, *Adv. Funct. Mater.* **2015**, *25*, 3698.
[9] K. I. Jang, H. U. Chung, S. Xu, C. H. Lee, H. W. Luan, J. Jeong, H. Y. Cheng, G. T. Kim, S. Y. Han, J. W. Lee, J. Kim, M. Cho, F. X. Miao, Y. Y. Yang, H. N. Jung, M. Flavin, H. Liu, G. W. Kong, K. J. Yu, S. I. Rhee, J. Chung, B. Kim, J. W. Kwak, M. H. Yun, J. Y. Kim, Y. M. Song, U. Paik, Y. H. Zhang, Y. Huang, J. A. Rogers, *Nat. Commun.* **2015**, *6*, 6566.
[10] L. B. Hu, H. S. Kim, J. Y. Lee, P. Peumans, Y. Cui, *ACS Nano* **2010**, *4*, 2955.
[11] F. Xu, Y. Zhu, *Adv. Mater.* **2012**, *24*, 5117.
[12] D. S. Hecht, L. B. Hu, G. Irvin, *Adv. Mater.* **2011**, *23*, 1482.
[13] P. C. Hsu, D. S. Kong, S. Wang, H. T. Wang, A. J. Welch, H. Wu, Y. Cui, *J. Am. Chem. Soc.* **2014**, *136*, 10593.
[14] P. Lee, J. Lee, H. Lee, J. Yeo, S. Hong, K. H. Nam, D. Lee, S. S. Lee, S. H. Ko, *Adv. Mater.* **2012**, *24*, 3326.
[15] P. C. Hsu, S. Wang, H. Wu, V. K. Narasimhan, D. S. Kong, H. R. Lee, Y. Cui, *Nat. Commun.* **2013**, *4*, 2522.
[16] P. Lee, J. Ham, J. Lee, S. Hong, S. Han, Y. D. Suh, S. E. Lee, J. Yeo, S. S. Lee, D. Lee, S. H. Ko, *Adv. Funct. Mater.* **2014**, *24*, 5671.
[17] G. F. Taylor, *Phys. Rev.* **1924**, *23*, 655.
[18] I. W. Donald, *J. Mater. Sci.* **1987**, *22*, 2661.
[19] I. W. Donald, B. L. Metcalfe, *J. Mater. Sci.* **1996**, *31*, 1139.
[20] Y. X. Li, D. Bergman, B. Zhang, *Anal. Chem.* **2009**, *81*, 5496.
[21] M. Bayindir, A. F. Abouraddy, J. Arnold, J. D. Joannopoulos, Y. Fink, *Adv. Mater.* **2006**, *18*, 845.
[22] D. S. Deng, N. D. Orf, S. Danto, A. F. Abouraddy, J. D. Joannopoulos, Y. Fink, *Appl. Phys. Lett.* **2010**, *96*, 023102.
[23] J. J. Kaufman, G. M. Tao, S. Shabahang, E. H. Banaei, D. S. S. Deng, X. D. Liang, S. G. Johnson, Y. Fink, A. F. Abouraddy, *Nature* **2012**, *487*, 463.
[24] S. J. Percival, N. E. Vartanian, B. Zhang, *RSC Adv.* **2014**, *4*, 10491.
[25] A. Gumennik, L. Wei, G. Lestoquoy, A. M. Stolyarov, X. T. Jia, P. H. Rekemeyer, M. J. Smith, X. D. Liang, B. J. B. Grena, S. G. Johnson, S. Gradecak, A. F. Abouraddy, J. D. Joannopoulos, Y. Fink, *Nat. Commun.* **2013**, *4*, 2216.
[26] H. L. Sorensen, E. S. Polzik, J. Appel, *J. Lightwave Technol.* **2014**, *32*, 1886.
[27] R. Romaniuk, *Bull. Pol. Acad. Sci: -Tech. Sci.* **2008**, *56*, 87.
[28] A. Cusano, M. Consales, A. Crescitelli, A. Ricciardi, *Lab-on-Fiber Technology*, Vol. *56*, Springer, New York, **2015**, pp. 1–26.
[29] J. A. Dantzig, M. Rappaz, *Solidification*, EPFL, Lausanne, **2009**, pp. 13–16.
[30] G. Chen, *Nanoscale Energy Transport and Converstion: A Parallel Treatment of Electrons, Molecules, Phonons and Photons*, Oxford University Press, Oxford, **2005**, pp. 233–242.
[31] N. Behabtu, C. C. Young, D. E. Tsentalovich, O. Kleinerman, X. Wang, A. W. K. Ma, E. A. Bengio, R. F. ter Waarbeek, J. J. de Jong, R. E. Hoogerwerf, S. B. Fairchild, J. B. Ferguson, B. Maruyama, J. Kono, Y. Talmon, Y. Cohen, M. J. Otto, M. Pasquali, *Science* **2013**, *339*, 182.
[32] S. Tawfick, K. O'Brien, A. J. Hart, *Small* **2009**, *5*, 2467.
[33] S. M. Ueland, *Materials Science and Engineering*, Massachusetts Institute of Technology, Cambridge **2009**.
[34] Y. Chen, X. X. Zhang, D. C. Dunand, C. A. Schuh, *Appl. Phys. Lett.* **2009**, *95*, 171906.
[35] J. Xiao, S. Y. Ryu, Y. Huang, K. C. Hwang, U. Paik, J. A. Rogers, *Nanotechnology* **2010**, *21*, 085708.

[36] F. R. Shanley, *J. Aeronaut. Sci.* **1947**, *14*, 261.
[37] L. Jin, A. Takei, J. W. Hutchinson, *J. Mech. Phys. Solids* **2015**, *81*, 22.
[38] W. W. Liang, M. Zhou, F. J. Ke, *Nano Lett.* **2005**, *5*, 2039.
[39] L. Pocivavsek, R. Dellsy, A. Kern, S. Johnson, B. H. Lin, K. Y. C. Lee, E. Cerda, *Science* **2008**, *320*, 912.
[40] H. Diamant, T. A. Witten, *Phys. Rev. Lett.* **2011**, *107*, 164302.
[41] J. J. Lao, D. Moldovan, *Appl. Phys. Lett.* **2008**, *93*, 093108.
[42] S. Hoffmann, I. Utke, B. Moser, J. Michler, S. H. Christiansen, V. Schmidt, S. Senz, P. Werner, U. Gosele, C. Ballif, *Nano Lett.* **2006**, *6*, 622.
[43] K. S. Kim, Y. Zhao, H. Jang, S. Y. Lee, J. M. Kim, K. S. Kim, J. H. Ahn, P. Kim, J. Y. Choi, B. H. Hong, *Nature* **2009**, *457*, 706.
[44] T. Yamada, Y. Hayamizu, Y. Yamamoto, Y. Yomogida, A. Izadi-Najafabadi, D. N. Futaba, K. Hata, *Nat. Nanotechnol.* **2011**, *6*, 296.
[45] Z. B. Yu, X. F. Niu, Z. T. Liu, Q. B. Pei, *Adv. Mater.* **2011**, *23*, 3989.
[46] Y. Y. Zhang, C. J. Sheehan, J. Y. Zhai, G. F. Zou, H. M. Luo, J. Xiong, Y. T. Zhu, Q. X. Jia, *Adv. Mater.* **2010**, *22*, 3027.
[47] T. Sekitani, H. Nakajima, H. Maeda, T. Fukushima, T. Aida, K. Hata, T. Someya, *Nat. Mater.* **2009**, *8*, 494.
[48] H. Wu, D. S. Kong, Z. C. Ruan, P. C. Hsu, S. Wang, Z. F. Yu, T. J. Carney, L. B. Hu, S. H. Fan, Y. Cui, *Nat. Nanotechnol.* **2013**, *8*, 421.